

Giant Coulomb broadening and Raman lasing on ionic transitions

A.A. Apolonsky, S.A. Babin, A.I. Chernykh, S.I. Kablukov,
S.V. Khorev, E.V. Podivilov, D.A. Shapiro

*Institute of Automation & Electrometry,
Novosibirsk, 630090, Russia*

CW generation of anti-Stokes Raman laser on a number of blue - green argon-ion lines (4p-4s, 4p-3d) has been demonstrated with optical pumping from metastable levels $3d' \ ^2G, 3d \ ^4F$. It is found, that the population transfer rate is increased by a factor of 3-5 (and hence, the output power of such Raman laser) owing to Coulomb diffusion in the velocity space. Measured are the excitation and relaxation rates for the metastable level. The Bennett hole on the metastable level has been recorded using the probe field technique. It has been shown that the Coulomb diffusion changes shape of the contour to exponential cusp profile while its width becomes 100 times the Lorentzian one and reaches values close to the Doppler width. Such a giant broadening is also confirmed by the shape of the absorption saturation curve.

42.55.Ye, 52.20.Hv, 32.70.Jz

I. INTRODUCTION

Stimulated Raman light scattering is widely used for frequency conversion of laser radiation [1]. Last years there is active development of CW anti-Stokes Raman lasers (ASRL) with frequency up-conversion that use two-photon inversion in active media of known lasers with gas-discharge excitation. CW generation of the ASRL was successfully achieved for the media of argon-ion [2], He-Ne [3] lasers and heavier noble atoms in electric discharge [4]. Conversion of radiation (648.3 nm→437.5 nm) in a 3-level Λ -scheme was studied [2] for ArII: $3d \ ^2P_{3/2} \rightarrow 4p \ ^2S_{1/2}^o \rightarrow 4s \ ^2P_{3/2}$. In the employed level scheme, a stepwise process

is dominant. That is, population transfer from metastable level $3d$ to upper laser level $4p$ takes place with subsequent emission on the $4p \rightarrow 4s$ transition. Despite the parameters of metastable level $3d^2P_{3/2}$ are not optimal (radiative lifetime of about 30 ns [5,6] is comparable with lifetimes of $4p$ -levels involved in laser transitions), the conversion efficiency appeared comparatively high ($> 50\%$). In particular, it was much higher than that in CW Raman lasers on atomic gases [3,4]. In the present paper, we study factors that can enhance output parameters of a Raman laser based on ions in a gas discharge plasma. In the comparatively dense and cold argon laser plasma the key role is played by Coulomb ion-ion collisions [7]. Collisions with velocity change effectively increase the number of particles that interact strongly with resonant radiation, and the longer the level's lifetime the larger increase in particle number there can be. Estimations indicate that metastables with lifetimes $\geq 10^{-7}$ s should have width of the hole "burnt" in the velocity distribution comparable to the Doppler width. This means that nearly all ions in metastable state interact with radiation.

In order to study collisional effects we achieved Raman generation on a number of transitions in Λ -configuration $3d \rightarrow 4p \rightarrow 4s(3d)$ starting from $3d'^2G, 3d^4F$ levels which have almost no radiative decay [5,6]. However, it is a fact that the metastable level relaxation in Ar^+ -laser plasma is determined by deactivation due to ion-electron collisions [7]. Corresponding figures for levels of interest are either unknown or there are contradictory data in different papers [8,9]. To carry out a quantitative analysis one has to measure both excitation and deactivation rates of the metastable level under real discharge condition. In this paper, we obtained relatively high output parameters of Raman laser without any optimization (even a plain linear resonator scheme allowed the up-conversion efficiency of more than 50% with respect to pump power, see section II). Since the population transfer rate and hence, the Raman laser output rely upon the metastable level excitation rate and fraction of the velocity distribution transferred to upper level, we concentrated at study of absorbing transition for a specific $3d'^2G_{7/2}$ level, aiming to clarify a role of collisions. We studied the absorption saturation (section III) and the nonlinear resonance in the probe field scheme brought about by the Bennett hole on the metastable level (section IV). Both experiments

show a giant broadening of the Bennett hole. Besides, the relaxation and excitation rates for the metastable level were extracted from the experimental data. We processed the acquired data using formulae from [10], which are valid for the simple two-level model. We modified them considering two aspects: difference between magnetic sublevels and longitudinal inhomogeneity of the fields in optically dense media. The formulae were checked against numerical simulation (section V), which accounted for deceleration due to dynamic friction force as well.

II. GENERATION OF THE ANTI-STOKES RAMAN LASER

In the present work, we have recorded the generation induced by optical pumping from the metastable to the upper laser level on a series of transitions:

$$\begin{aligned}
&610.4 \rightarrow 457.9 \text{ nm } (3d \ ^2P_{1/2} \rightarrow 4p \ ^2S_{1/2}^o \rightarrow 4s \ ^2P_{1/2}),^* \\
&648.3 \rightarrow 457.9 \text{ nm } (3d \ ^2P_{3/2} \rightarrow 4p \ ^2S_{1/2}^o \rightarrow 4s \ ^2P_{1/2}),^* \\
&613.9 \rightarrow 496.5 \text{ nm } (3d \ ^4F_{5/2} \rightarrow 4p \ ^2D_{3/2}^o \rightarrow 4s \ ^2P_{3/2}), \\
&624.3 \rightarrow 488.0 \text{ nm } (3d \ ^4F_{7/2} \rightarrow 4p \ ^2D_{5/2}^o \rightarrow 4s \ ^2P_{3/2}), \\
&617.2 \rightarrow 501.7 \text{ nm } (3d' \ ^2G_{7/2} \rightarrow 4p' \ ^2F_{5/2}^o \rightarrow 3d \ ^2D_{3/2}).
\end{aligned}$$

The schematic diagram of the experimental setup is presented in fig. 1. We used the output of a single-frequency linearly polarized dye laser as the pump source. The pump radiation wavelength was controlled by a λ -meter with 10^{-3} nm resolution. This was done using a fraction of the pump beam reflected by mirror M_1 . The main beam was directed by mirror M_2 and further focused by lense L into the discharge tube propagating along the discharge through mirror M_3 of the argon laser which had a low reflectance in the red spectrum range. The cavity of the main laser consisted of mirrors M_3 and M_4 . In the absence of pump beam, a usual series of well-known ArII lines was observed. Owing a relatively large transmittance ($5 \div 10\%$) of mirror M_4 in the green-blue region, weak lines 457.9, 496.5 and 501.7 nm had low gain-to-loss ratio. Under such conditions, the fraction of output power that came from the optical pump was substantially larger than the usual

lasing. The output lines were separated by prism Pr . Aperture spot D_2 served to select the TEM₀₀ generation mode of the argon laser and, together with D_1 maintained the pump and Raman generation beams coaxiality, which simplified alignment a lot. In our experiments, we employed an argon ion laser with longitudinal gas flow, in order to achieve a highly longitudinal uniformity of the discharge [11]. 7 mm-bored discharge tube was 1 m in length, it operated at current of 100 A, the pressure being set optimally for argon laser generation. These parameters were used throughout this work.

The scheme of generation on starred transitions is almost the same as in [2], i.e. same starting levels are used: $3d\ ^2P_{1/2}, 3d\ ^2P_{3/2}$. Using instead of 437.5 nm line the 457.9 nm one that has a larger Einstein coefficient, we obtained comparable to that of [2] conversion efficiency (output power exceeded 30% of pump power), even in a plain linear scheme of Raman laser. Farther, in the scheme with metastables $^2G, ^4F$, the efficiency was comparable to or higher than in [2] (up to 60%).

For a detailed study, we chose the scheme with the largest pump radiation absorption ($3d'\ ^2G_{7/2} \rightarrow 4p'\ ^2F_{5/2}^o \rightarrow 3d\ ^2D_{3/2}$), see fig. 1. In the study of Raman generation on this transition, we carried out spectral measurements of the 501.7 nm line with the scanning interferometer SI (5 GHz free dispersion range) and photodiode PD connected to an oscilloscope. In the absence of optical pumping, we observed generation on 501.7 nm near the threshold, the line averaged gain coefficient under these conditions amounted to about $\sim 10\%$, only a narrow part of the gain contour about the line center was above the threshold, a noise spectrum with the width of about 1 GHz being recorded with random jumps among adjacent laser modes. Under a single-frequency optical pumping on the 617.2 nm line an additional narrow peak of Raman generation appeared. The noisy background disappeared when the peak was tuned into the line center. At the pump power of 70 mW we observed that the Raman peak shifts in correspondence with detuning of the pump radiation and is present in the output up to at least ± 4 GHz detuning. That is, even under such detunings, the gain coefficient exceeded 10% (induced by the optical pump). This indicates a possibility to optimize the system applying techniques of multi-mirror resonators as described in [2],

and produce a high output power having a broad tunable range.

III. ABSORPTION SATURATION

For absorption measurements the scheme of fig. 1 was used, but mirror M_4 was removed, and hence, no generation occurred. Lens L was chosen so that it formed a beam only slightly diverging along the discharge tube. The pump beam was attenuated with a set of filters and the transmitted intensity was registered. The passed through power was normalized to the average beam crosssection $S = (0.44 \pm 0.05) \text{ mm}^2$ and thus the average intensities I_i and I_f at the entrance to and at the exit from the discharge tube, correspondingly.

The saturation behavior of absorbed power for ionic transitions is strongly dependent on diffusion in velocity space owing to Coulomb collisions [7,10]. Given the ion density $N_i = N_e \simeq 1.7 \times 10^{14} \text{ cm}^{-3}$ and the temperature $T_i = m_i v_T^2 / 2 \simeq 1 \text{ eV}$, which correspond to the experimental conditions, the effective frequency of ion-ion collisions amounts to $\nu_{ii} \simeq 2 \times 10^7 \text{ c}^{-1}$ [7] and corresponding diffusion coefficient is $D \simeq 5 \times 10^{17} \text{ cm}^2 \text{ c}^{-3}$

$$\nu_{ii} = \frac{16\sqrt{\pi}N_i e^4 \Lambda}{3m_i^2 v_T^3}, \quad D = \frac{\nu_{ii} v_T^2}{2} \quad (1)$$

where Λ is the Coulomb logarithm, e is the electron charge, m_i is the ion mass. It is shown in [10] that at strong diffusion the saturation of the absorbed power P per unit volume versus the field intensity $I = 16\pi^2 \hbar c |G|^2 / \lambda^3 A_{mn}$, ($|G|^2 = |Ed_{mn}/2\hbar|^2$ is Rabi frequency) has a homogeneous form:

$$P = \frac{2\hbar\omega\sqrt{\pi}(N_n(g_m/g_n) - N_m)}{kv_T} \frac{|G|^2}{1 + |G|^2/|G_s|^2}, \quad (2)$$

$$|G_s|^2 = \frac{\sqrt{2\nu_{ii}}kv_T}{2\pi} \left(\frac{1}{\sqrt{\Gamma_m}} + \frac{1}{\sqrt{\Gamma_n}} \right)^{-1} \quad (3)$$

The formula is valid up to intensities determined by condition $kv_T\sqrt{\nu_{ii}/2\Gamma_n} \gg |G|\sqrt{\Gamma_{mn}/\Gamma_n}$, meaning that diffusional width exceeds homogeneous one (including field broadening). The results of [10] were obtained under assumption that

$$kv_T \gg \Gamma_n, \Gamma_m, \Gamma_{mn}, \Omega; \quad \nu_{ii}(kv_T)^2/\Gamma_{mn}^3 \ll 1; \quad (4)$$

where $\Omega = \omega - \omega_{mn}$ is the difference between the radiation frequency and the Bohr frequency of the $m-n$ transition, Γ_j are relaxation constants for the levels, $\Gamma_{mn} = (\Gamma_m + \Gamma_n)/2$. The latter condition holds well for the laser ArII lines. In our case, this is not valid, since the metastable relaxation constants Γ_n are much less than those of the laser levels. Provided the radiation is linearly polarized, we can neglect the degeneracy and treat the $3d'^2G_{7/2} \rightarrow 4p'^2F_{5/2}^o$ transition as a two-level system taking into consideration the degeneracy factors $g_{m,n} = 2J_{m,n} + 1$ of upper (m) and lower (n) levels. To check for validity of expression (2), (3) for concrete levels we compared them with numerical solution of the equations for the density matrix (see Sec. V).

As long as up to 90% of the incident radiation is absorbed, it is necessary to consider the optical density of the medium. In such case the relation between the incident (I_i) and output (I_f) intensities has the form:

$$\ln\left(\frac{I_i}{I_f}\right) + \frac{I_i - I_f}{I_s} = k_o l, \quad (5)$$

where the small-signal absorption coefficient has usual form

$$k_o \simeq \frac{\lambda^3 A_{mn}}{8\pi^{3/2} v_T} (N_n(g_m/g_n) - N_m), \quad (6)$$

and the saturation intensity is

$$I_s = \frac{8\pi\sqrt{2\nu_{ii}}kv_T\hbar c}{\lambda^3 A_{mn}} \left(\frac{1}{\sqrt{\Gamma_m}} + \frac{1}{\sqrt{\Gamma_n}} \right)^{-1}. \quad (7)$$

In the fig. 2, the dependence of the absorption $\Delta I = I_i - I_f$ on the incident intensity I_i given by the expression (5) is plotted along with the experimental points according to maximum-likelihood fit. The extracted values of the unsaturated absorption coefficient $k_o = (2.14 \pm 0.05) \times 10^{-2} \text{ cm}^{-1}$, and saturation intensity $I_s = 11.2 \pm 2.1 \text{ W/cm}^2$. A comparison between the absorption on this transition and the gain coefficient for the adjacent transition 501.7 nm indicated that the metastable level $3d'^2G_{7/2}$ population is 14 times the $4p'^2F_{5/2}^o$ level population. Knowing the Einstein coefficient for this transition $A_{mn} = 2.2 \times 10^7 \text{ s}^{-1}$

[6] and the discharge length being $l = 100\text{cm}$, one can obtain the lower level population $N_n \simeq (5.33 \pm 0.14) \times 10^{10} \text{ cm}^{-3}$ from formula (6). One can also determine the lower level decay rate with the help of Eq.(7). The upper level decay rate was taken from literature: $\Gamma_m = 2.0 \times 10^8 \text{ c}^{-1}$ ($\tau_m = 8.4 \text{ ns}$ – radiative lifetime [6], $K_m \simeq 10^{-7} \text{ cm}^3 \text{ c}^{-1}$ is the deactivation constant [13]). The obtained lower level lifetime is $\Gamma_n \simeq (7.7 \pm 4.6) \times 10^7 \text{ c}^{-1}$, the low accuracy is owing to the fact that only slight saturation was achieved. Additional error is introduced by uncertainty in the measured saturation intensity caused by transverse nonuniformity of the beam. Since the expression for Γ_n includes a difference of two very close values, the calculated result is rather an estimation. Measuring the width of the nonlinear resonance in the spectrum of the probe field one can determine more accurately the metastable level relaxation constant. As soon as the contribution of the levels m and n into the nonlinear resonance is inversely proportional to Γ_j , one can draw a conclusion, on the basis of the yielded results, that the contribution of the lower level is at least 3 times greater than that of the upper one. The measurements of the nonlinear resonance shapes are covered in the next section.

IV. NONLINEAR RESONANCE

The scheme of the experiment on nonlinear resonance measurements in the probe field spectrum is presented in fig. 3. To split the dye laser beam into two, the pump beam and the probe one (a and b in fig. 3, correspondingly), we used a reflection from the uncoated surface of the output mirror (M_1 in fig. 3). The probe beam power amounted to a few percent of the strong one. Lenses L_1 and L_2 were used to ensure minimal divergence of the beams along the discharge tube, the diameter of the probe beam being 3 times smaller than that of the pump beam. The passed through the discharge probe beam was detected behind the beam splitter BS_2 (transmittance $t \sim 20\%$). Lock-in detector Unipan 232B was used. A fraction of the pump beam coming through the splitter BS_1 and modulated by chopper Ch was used as the reference signal. Chopper in position 1 modulates both beams, and the

lock-in detector registers the transmitted through the discharge power of the probe beam. Placed in position 2, the chopper affects the pump beam only, and the lock-in detector registers variation of the passed through probe power occurring due to influence of the pump beam. The intensity of the pump field was measured with an account for change in the dye laser beam cross-section. To do this an additional registration of variation in intensity near the beam axis was made using an aperture stop D (the diameter is much smaller than the effective beam diameter). The frequency detuning was measured with scanning interferometer SI , photodiode PD and oscilloscope Os . Along with the dye laser frequency the scanning interferometer registered the single-frequency He-Ne laser signal. The latter served as a reference point to detuning of the dye laser.

Owing to a strong absorption, the depth of the “burnt” Bennett hole changes along the discharge. That’s why we need a formula for the resonance in an optically dense medium. Neglecting the influence of the probe field I_1 on the strong one I_2 which propagates towards I_1 in the opposite direction from the point $z = l$ to $z = 0$, we have an exponential intensity dependence on the linear distance z : $I_2(z) = I_2(l) \exp [k(\Omega_2)(z - l)]$. The corresponding dependence of the weak field intensity $I_1(z)$ can be extracted from the following equation, taking into account a weak saturation of the transition by the strong field $I_2(z)$:

$$\frac{dI_1(z)}{dz} = -k(\Omega_1) \cdot I_1(z) \left(1 - F(\Omega_1, \Omega_2) \frac{I_2(z)}{I_s} \right), \quad (8)$$

where $\Omega_{1,2}$ are frequency detuning of the weak and strong fields from the exact resonance correspondingly;

$$F(\Omega_1, \Omega_2) \simeq \exp \left(-\frac{|\Omega_2 - \Omega_1|}{kv_T} \sqrt{\frac{2\Gamma_n}{\nu_{ii}}} \right) \quad (9)$$

where F is the function that describes the shape of the Bennett hole in case of diffusion broadening (see review [7] and references therein, validity of the expression as applied to the studied transition is discussed in Section V). In the investigated scheme $\Omega_1 = -\Omega_2 = \Omega$, thus velocities of particles resonant to probe and pump field $\pm\Omega/k$ only differ in sign).

The solution of Eq.(8) can be written in the following form:

$$F_{1,2} = F(\Omega, -\Omega) \simeq \frac{I_s(I_1(l) - \tilde{I}_1(l))}{I_2(l)\tilde{I}_1(0)(1 - \exp(-k(\Omega)l)) \exp(-k(\Omega)l)}, \quad (10)$$

where $\tilde{I}_1(l) = \tilde{I}_1(l) \exp(-k(\Omega)l)$ is the probe field intensity in the absence of the strong field, i.e. at $I_2 = 0$.

In the experiments, the readings of the lock-in detector were recorded when the chopper *Ch* was in position 2; in this case they were proportional to $I_1(l) - \tilde{I}_1(l)$. The input intensities of the probe $\tilde{I}_1(0)$ and pump $I_2(l)$ fields were proportional to the output power of the dye laser. With the chopper in position 1 we measured the dependence of the absorption coefficient upon detuning $k(\Omega) = k_o \exp(-\Omega^2/(kv_T)^2)$. From these data we reconstructed $F_{1,2}$ as a function of detuning Ω up to an arbitrary amplitude. The dependence calculated in this way is demonstrated in fig. 4. It's relevant to mention that the experimental data consist of two overlapping sets of points, because it was difficult to cover the required range in one sweep. Experimental points were approximated by expression (9) using the maximum-likelihood fit. Three parameters were fitted: magnitude, width and detuning zero shift.

The processed data yielded diffusion full width at half a maximum (FWHM) $\Delta = (\ln 2/\pi)\sqrt{\nu_{ii}/2\Gamma_n}kv_T = (3.0 \pm 0.3)$ GHz, the Doppler width (FWHM) being $\Delta\nu_D = kv_T\sqrt{\ln 2}/\pi = (5.3 \pm 0.1)$ GHz. Internal noises of the dye laser in the vicinity of the strong field chopping frequency can lead to systematic error, that is, the total error can exceed 10%. The decay rate of the metastable level extracted from the diffusion width is $\Gamma_n = (2.3 \pm 0.5) \times 10^{-7}\text{c}^{-1}$, which agrees with the value obtained from saturation intensity. Hence, our assumptions concerning contributions of the upper and lower levels into the resulting contour of the nonlinear resonance are obviously true, $\Gamma_n \simeq 0.1\Gamma_m$. To compare the Bennett hole width and that of the Doppler contour, we showed in the inset to fig. 4 the corresponding velocity distributions at zero detuning from exact resonance. We should take into account that the Bennett hole width is Δ and the width of function $F_{1,2}$ in Eq.(9) is $\Delta/2$ which comes from scanning the hole with double speed. It is seen from the plot that collisions “blur” the Bennett hole to almost fill the whole Doppler contour.

Besides, knowing the relaxation rate and population we find that the excitation rate of the metastable level Q_n 1.6 times greater than that of the upper laser level.

V. NUMERICAL SIMULATION

As soon as not all the assumptions made in [10] hold in case of our investigations, we had check for accuracy of the analytical expressions. To do this we carried out a numerical solution of the equation array for the density matrix of a two-level system in the field of a running electromagnetic wave including Coulomb diffusion and dynamic friction force. The array to solve follows [7]:

$$\begin{aligned}
(\Gamma_{mn} - i\Omega + ikv)\rho_{mn} - \hat{D}\rho_{mn} &= -iG(\rho_{mm} - \rho_{nn}), \\
\Gamma_m\rho_{mm} - \hat{D}\rho_{mm} &= Q_m W(v) - 2\mathbf{Re}(iG^* \rho_{mn}), \\
\Gamma_n\rho_{nn} - \hat{D}\rho_{nn} &= Q_n W(v) + 2\mathbf{Re}(iG^* \rho_{mn});
\end{aligned} \tag{11}$$

where

$$\hat{D}\rho_{ij} = \nu_{ii} \frac{\partial}{\partial v}(v\rho_{ij}) + \frac{1}{2}\nu_{ii}v_{\text{T}}^2 \frac{\partial^2}{\partial v^2}\rho_{ij}, \tag{12}$$

Q_j is total excitation rate of j -th level, $W(v)$ is one-dimensional Maxwell distribution over velocity having width v_{T} . We neglected terms proportional to A_{mn} , since they are small ($A_{mn} \simeq 0.1\Gamma_m$) for the studied transition. For the numerical solution of Eq.(11) at pre-set parameters in operator \hat{D} symmetrical differences were substituted for partial velocity derivatives. At $v = 5v_{\text{T}}$ we took the asymptotic condition $\rho = 0$, and solved the resulting array of linear algebraic equations using the matrix sweep method. To calculate the field work and the shape of the nonlinear resonance, we averaged over velocities the produced distribution for $\rho_{ij}(v)$ using formalism given in [7].

Different behavior of the magnetic sublevels was taken into consideration, too. When a linearly polarized field interacts with transition $3d'^2G_{7/2} \rightarrow 4p'^2F_{5/2}^o$ only allowed transitions are those preserving the projection of magnetic momentum M onto the polarization

direction. Magnetic sublevels with the same projection M can be regarded as independent two-level subsystems with different dipole moments:

$$|d_M|^2 = |\langle m||d||n\rangle|^2 \left| \begin{pmatrix} 7/2 & 5/2 & 1 \\ M & -M & 0 \end{pmatrix} \right|^2 \quad (13)$$

where $\langle m||d||n\rangle$ is the normalized dipole moment,

$$|d_{5/2}|^2 = \frac{3}{28} \frac{|\langle m||d||n\rangle|^2}{3}; |d_{3/2}|^2 = \frac{5}{28} \frac{|\langle m||d||n\rangle|^2}{3}; |d_{1/2}|^2 = \frac{3}{14} \frac{|\langle m||d||n\rangle|^2}{3} \quad (14)$$

At a given intensity I , the field magnitude (in frequency units) $|G_M|^2 = |Ed_M/2\hbar|^2$ is different for every subsystem. The absorbed power is found by summing up over all subsystems. For each of them expression (2) is valid with the substitution $|G|^2 \rightarrow |G_M|^2$ and $[(g_m/g_n)N_n - N_m] \rightarrow [(N_n/g_n) - (N_m/g_m)]$. At low and high intensities $I \ll I_s$ and $I \gg I_s$, the total absorption is exactly the same as that of a two-level system according to Eq.(2). The largest deviation is achieved at $I = I_s$ and does not exceed to 2%.

Numerical calculations were carried out for values for the population of the metastable level acquired in experiments on absorption saturation, and values for the upper level population from measurements of the gain coefficient of a laser line on the adjacent transition. The metastable level decay rate was taken from experiment with nonlinear resonance in the probe field scheme.

In fig. 5a, a comparison between the dependence of absorbed power P per unit volume upon field intensity I_i for a two-level system in an optically thin medium according to Eq.(2) (the dotted line) and that calculated on a PC with an account for dynamic friction and specific values for dipole moments of magnetic sublevels (14) (the solid curve). As can be seen from fig. 5a, the difference between the two curves is within 5%. This means that dynamic friction is the main source of discrepancy. Besides, the numerical data at given values $\Gamma_j, Q_j, A_{mn}, \nu_{ii}, v_T$ can be fitted by the analytical expression $P = k_o I / (1 + I/I_s)$, but with different values for k_o, I_s . The yielded fit parameters are lower by 2% and 6% correspondingly than k_o, I_s in (6) and (7).

The contour of the nonlinear resonance $\Delta k(\Omega)$ was calculated numerically for intensity of the strong field $I_2 = 0.1I_s$, and probe field intensity $I_1 \ll I_s$ in accordance with the experimental conditions. In fig. 5b, the solid curve is for numerical calculations and the dashed line is for analytical approximation $\Delta k(\Omega) = F_{1,2} \exp(-\Omega^2/(kv_T)^2)I_2/I_s$ used for experimental data processing. It deviates from the numerical simulation by a factor of 1.45 with an accuracy not worse than 3% over all the detuning range, i.e. copies the resonance shape.

VI. DISCUSSION

We analyzed the dependence of absorption upon pump field intensity, as well as the nonlinear resonance that comes from the Bennett hole on the metastable level. This included approximation of the experimental values with analytical expression and a comparison of the theory with the numerical solutions of the equation array for the density matrix. As a result, it was clearly demonstrated that both the shape of the saturation curve and shape of the Bennett hole are primarily a consequence of Coulomb diffusion of ions in the velocity space. The diffusion leads to an abnormal broadening of the Bennett hole: diffusional width of the hole Δ for the metastable $3d'^2G_{7/2}$ reaches 3 GHz, whereas Lorentzian width of the transition Γ_{mn}/π amounts to as little as 35 MHz. This means that is a relative broadening by a factor of nearly 100. With the field broadening included, the transition width $\Gamma_{mn}\sqrt{1 + 4|G|^2/\Gamma_m\Gamma_n} \sim 10\Gamma_{mn}$ is also much less than the diffusional one. Thus, the giant Coulomb broadening completely determines the character of saturation on the transition. Instead of the well-known “hole burning” in the velocity distribution one observes nearly complete saturation of the whole Doppler contour. The form of the saturation resonance has an unusual exponential cusp feature (see fig. 4). It’s relevant to note that such exponential wings were observed in the spectrum of the probe field on transition $3d'^2G_{9/2} \rightarrow 4p'^2F_{7/2}$ of argon ion under conditions of hollow cathode discharge [9,14]. The authors of these papers attributed the broadening to ion-atom collisions. Unfortunately, plasma parameters

were not measured and this is a serious obstacle to quantitative analysis. However, despite considerable difference in plasma parameters (specifically, much lower charged particle concentrations in hollow cathode), Coulomb collisions may also play a noticeable role there.

Coulomb broadening changes completely the form of the saturation curve. The typical for single-frequency pumping inhomogeneous saturation $k_o/\sqrt{1 + |G|^2/|G_o|^2}$ gets substituted by homogeneous saturation: $k_o/(1 + |G|^2/|G_s|^2)$. The saturation intensity differs by a factor of 60 for these cases. The dotted lines in fig. 2 correspond to inhomogeneous saturation and to the asymptote of the maximum absorbed power $P \simeq (6/8)Q_n\hbar\omega Sl$ (the expression holds when $\Gamma_n \ll \Gamma_m$). At intensities used in our experiments, the curve that takes Coulomb diffusion into account saturates noticeably nearing the asymptotic value, whereas the inhomogeneous saturation curve is far from this. At pump intensities $I \sim I_s$ diffusion results in absorption increase (and hence, the output power of the Raman laser on the adjacent transition) by a factor 3–5 depending on specific values of relaxation constants. Note, that the perturbation influence of Raman generation on absorption of the pump radiation is small in case $\Gamma_n \ll \Gamma_m$. At low intensities (much lower than the saturation intensity on the adjacent transition) the generation repeats the dependence of absorbed power on the pump input. We should mention that earlier [15], simple formulae for the output power of Raman laser using perturbation method in the pump and generation fields were already written that qualitatively demonstrate the role played by Coulomb diffusion.

Let's compare the obtained value for the relaxation constant of the metastable level $\Gamma_n \simeq 2 \times 10^7 \text{ c}^{-1}$ with data found in other papers. We know no published figures for level $3d'^2G_{7/2}$ deactivation in plasma, however there are some results on the similar metastable level $3d'^2G_{9/2}$. In [8], the laser induced fluorescence was observed in a hollow cathode discharge. The measured electron deactivation coefficient appeared to be $(2.5 \pm 1.0) \times 10^{-8} \text{ cm}^3/\text{c}$, electron temperature being $T_e = 3.5 \text{ eV}$. For electron density $N_e \simeq 2 \times 10^{14} \text{ cm}^{-3}$, which corresponds to our experiments, we get the decay rate $\Gamma_n \sim 5 \times 10^6 \text{ c}^{-1}$. In [9], there is the relaxation constant of the metastable level $3d'^2G_{9/2}$ $\Gamma_n \sim 10^8 \text{ c}^{-1}$, again for a hollow cathode discharge. Authors of Ref. [9] supposed that metastable is quenched due to resonant

charge-exchange collisions of excited argon ions with atoms in ground state. Estimations for electron deactivation of level $3d'^2G_{7/2}$ that take into consideration only the predominant channel $3d'^2G_{7/2} \rightarrow 4p'^2F_{5/2}^o$ done in Bates-Damgaard approximation (using tables in the book by Vainshtein et. al. [16]) yields $\Gamma_n \simeq 4 \times 10^6 \text{c}^{-1}$, which is slightly lower than the measured value. Probably, in our conditions relaxation occurred due to both collisions with electron and resonant charge-exchange with neutrals. This shows that the experimental value for the relaxation rate $\Gamma_n \simeq 2 \times 10^7 \text{c}^{-1}$ of level $3d'^2G_{7/2}$ does not contradict to estimations and lies within scatter of data in [8,9] for the relaxation rate of the similar level $3d'^2G_{9/2}$.

Note, that the studied metastable level has the relaxation rate comparable with ion-ion collision frequency. Under such conditions the dynamic friction force and velocity dependence of the diffusion coefficient can lead to a noticeable narrowing of the Bennett hole centered at a wing of velocity distribution $v > v_T$ [17]. Experiments with independently tuned strong and probe fields may test the phenomenon.

VII. CONCLUSION

1. The present work has demonstrated the possibility of Raman generation due to an optical pumping from metastable levels $3d'^2G, 3d^4F$ on a number of generation lines of argon laser.

2. For absorbing transition $3d'^2G_{7/2} \rightarrow 4p'^2F_{5/2}^o$ of the Raman laser $617.2 \rightarrow 501.7 \text{ nm}$, the unsaturated absorption coefficient $k_o = 2 \times 10^{-2} \text{ cm}^{-1}$, and saturation intensity $I_s = 11 \text{ W/cm}^2$ have been determined.

3. The ratios of populations (~ 14) and excitation rates (~ 1.6) for levels $3d'^2G_{7/2}$ and $4p'^2F_{5/2}^o$ have been measured. The relaxation rate of level $3d'^2G_{7/2}$ $\Gamma_n = 2.3 \times 10^{-7} \text{c}^{-1}$ is determined primarily by collisional deactivation in plasma.

4. The Bennett hole on metastable level $3d'^2G_{7/2}$ is broadened by a factor of 100 owing to Coulomb collisions. The hole has exponential shape and its width $\Delta \sim 3 \text{ GHz}$ is comparable to the Doppler one. This giant broadening is the key factor in the character of saturation on

the transition. Instead of usual “hole burning” in the velocity distribution, we observed an almost complete saturation of the whole Doppler contour. This adds up to the population transfer to the upper level and hence, to the efficiency of the Raman laser.

ACKNOWLEDGEMENTS

The authors are grateful to S.M. Kobtsev for technical assistance and to E.A. Yukov for fruitful discussions.

The present paper has been partially sponsored by the International Science Foundation and Russian Government, grant RCN 300.

-
- [1] J.C.White, Topics in Applied Physics **59**, 115 (1989).
 - [2] A. Feitish, D. Schnier, T. Müller, B. Wellegehausen, IEEE J. Quantum Electron. **24**, 507 (1988); B. Wellegehausen, CLEO/IQEC, 1990.
 - [3] K. Rittner, A. Höpe, T. Müller-Wirts, B. Wellegehausen, IEEE J. Quantum Electron. **28**, 342 (1992).
 - [4] K. Rittner, A. Wicht, G. Jordan, A. Heuer, H. Welling, B. Wellegehausen, Laser Physics **4**, 339 (1994).
 - [5] B.F. Luyken, Physica **60**, 432 (1972).
 - [6] A. Hibber, J. Hansen, J. Phys.B **27**, 3325 (1994).
 - [7] S.A. Babin, D.A. Shapiro, Phys. Rep. **241**, 119 (1994).
 - [8] H.M.I. Willems, K. Yuasa, B. van der Sijde, D.C. Schram, J.A.M. van der Mullen, J. Quant. Spectrosc. Radiat. Transfer **41**, 251 (1989).
 - [9] M. Elbel, M. Simon, H. Welp, Quantum Optics **2**, 351 (1990).

- [10] K.B. Kurlayev, D.A. Shapiro, *Kvant. Elektron* **21**, 1080 (1994), [*Sov. J. Quantum Electron.* **24**, 1003 (1994)].
- [11] S.A. Babin, A.E. Kuklin, *Proc. SPIE* **1397**, 589 (1991).
- [12] A.D. White, E.I. Gordon, J.D. Rigden, *Appl. Phys. Lett.* **2**, 91 (1963).
- [13] J. Jolly, *J. Quant. Spectrosc. Radiat. Transfer.* **20**, 503 (1978).
- [14] W. Bestgen, M. Elbel, R. Lange, H. Welp, *J. Phys.B* **28**, 2575 (1995).
- [15] S.A. Babin, S.G. Rautian, D.A. Shapiro, *Kvant. Elektron.*, **19**, 1139 (1992), [*Sov. J. Quantum Electron.* **22**, 1065 (1992)].
- [16] I.I. Sobelman, L.A. Vainshtein, E.A. Yukov, *Excitation of atoms and Broadening of Spectral lines* (Springer, Berlin, 1981).
- [17] E.V. Podivilov, D.A. Shapiro, M.G. Stepanov, *Phys. Rev. Lett.* **72**, 3979 (1995).

LIST OF CAPTIONS

Fig. 1. Experimental setup for the study of Raman generation: M_1 – low-reflectance mirror; M_2 – high-reflectance turning mirror; λ -meter – wavelength controller, L_1 – lens; D_1, D_2 – aperture stops; M_3, M_4 – argon laser cavity mirrors; Pr – dispersion prism; SI – scanning interferometer; PD – photo detector. There is a scheme of levels involved in Raman generation in this figure.

Fig. 2. Dependence of the absorbed intensity $\Delta I = I_i - I_f$ on the transition $3d' ^2G_{7/2} \rightarrow 4p' ^2F_{5/2}^o$ upon the incident intensity I_i . Boxes correspond to experimental data. Theoretical dependence (solid curve) (5) is fitted with the maximum-likelihood algorithm. Dots correspond to inhomogeneous saturation with Coulomb diffusion neglected. The straight lines correspond to the derivative from the saturation curves at zero intensities, and to the asymptote of maximum possible absorption. (Discharge length 100 cm, electron density $N_e \simeq 1.7 \times 10^{-14} \text{cm}^{-3}$, electron and ion temperatures $T_e \simeq 4 \text{eV}$, $T_i \simeq 0.8 \text{eV}$, respectively).

Fig. 3. Experimental setup for study of nonlinear resonance in the probe field configuration: M_1 – coupling mirror of dye laser, M_2, M_3, M_4, M_5 – beam turning mirrors, BS_1, BS_2 – beam splitters, L_1, L_2 – focusing lenses, Lock-in – lock-in detector, Ch – beam chopper, D – small aperture stop. Letters a and b mark pump and probe beam paths correspondingly. Chopper in position 1 modulates both pump and probe fields, in position 2 it only effects the pump beam. The scanning interferometer (SI), photo detector (PD), oscilloscope (OS) and single-frequency He-Ne laser are the components of the spectrum analyzer.

Fig. 4. Function (10) $F_{1,2}$ versus detuning $\Omega/(2\pi)$ (in GHz) fitted into the experimental points by maximum-likelihood method. Crosses and boxes are for two different data sets. The discharge parameters are the same as in the experiment on saturation measurement. For comparison, the Doppler velocity distribution (in v_T units) and the shape of the Bennett hole on the metastable level are also shown.

Fig. 5. a – Dependence of the absorbed power P upon field intensity I_i in an optically thin medium for a two-level system (2) and a numerical simulation (11) for magnetic sublevels

with friction force included (dashed and solid curves correspondingly). b – The variation of the absorption coefficient $\Delta k(\Omega) = F_{1,2} \exp(-\Omega^2/(kv_T)^2)I_2/I_s$ caused by the strong field at the intensity $I_2 = 0.1I_s$: solid curve plots the results of numerical simulation, dashed curve is the analytical approximation (parameters taken from experiments).

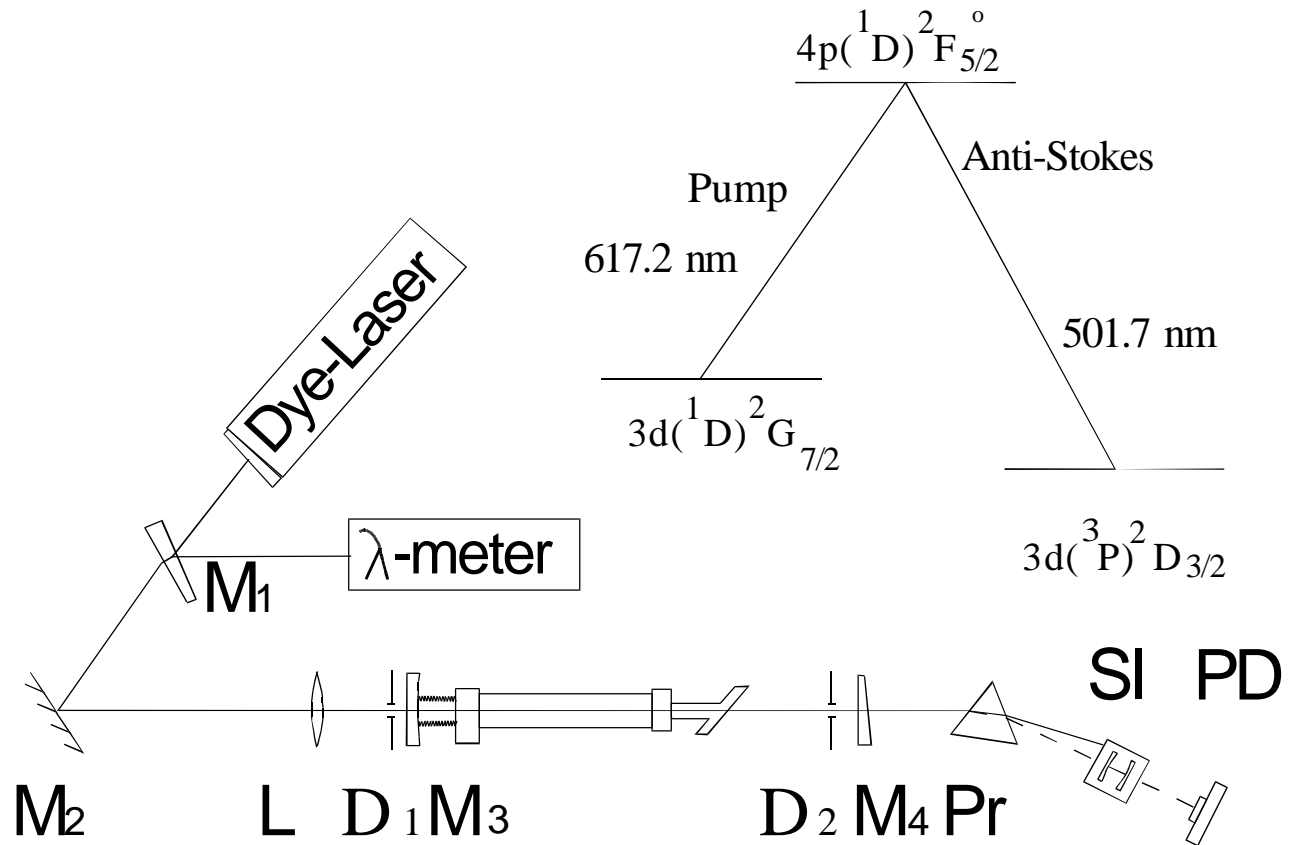


Fig.1

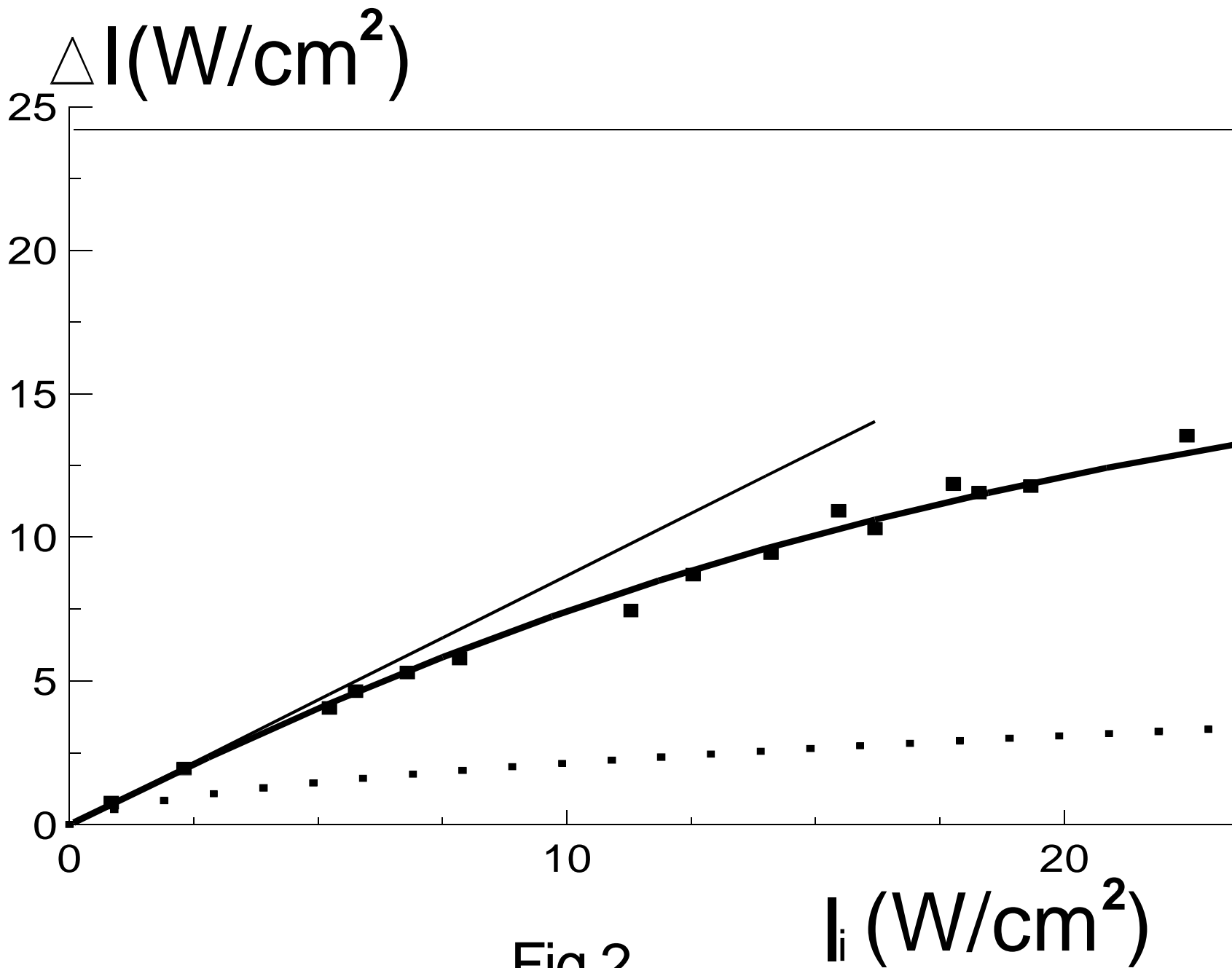


Fig.2

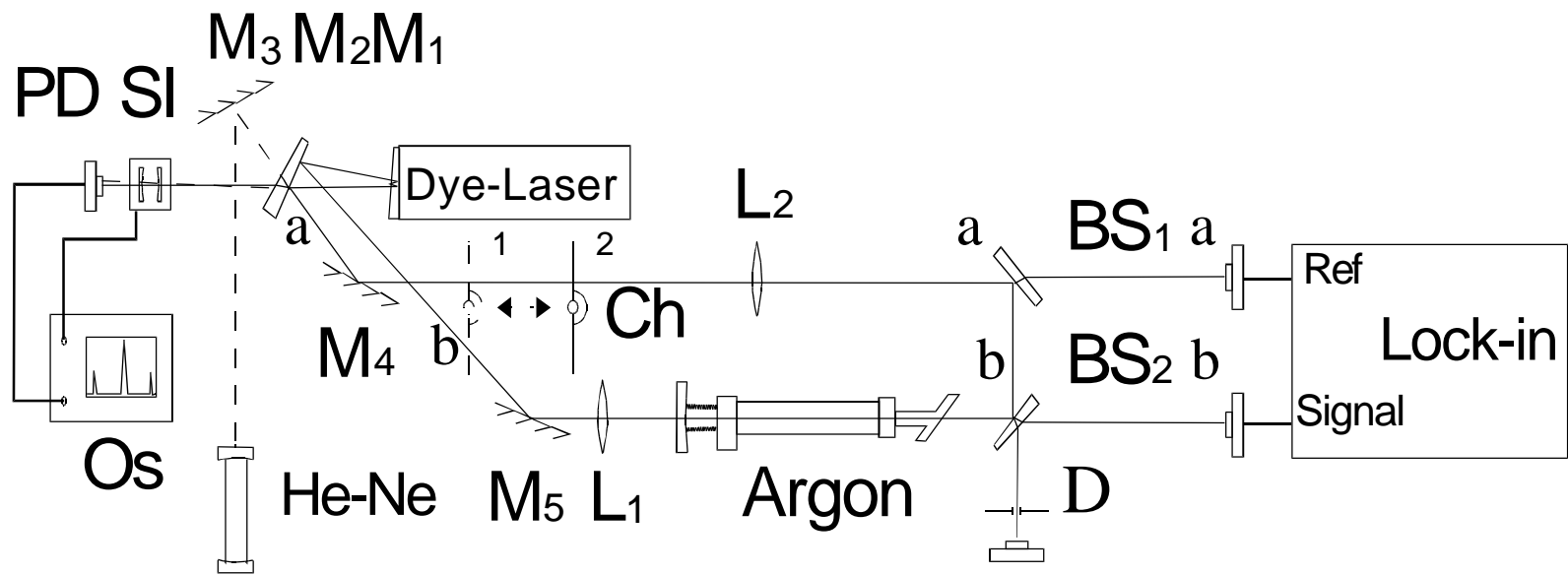
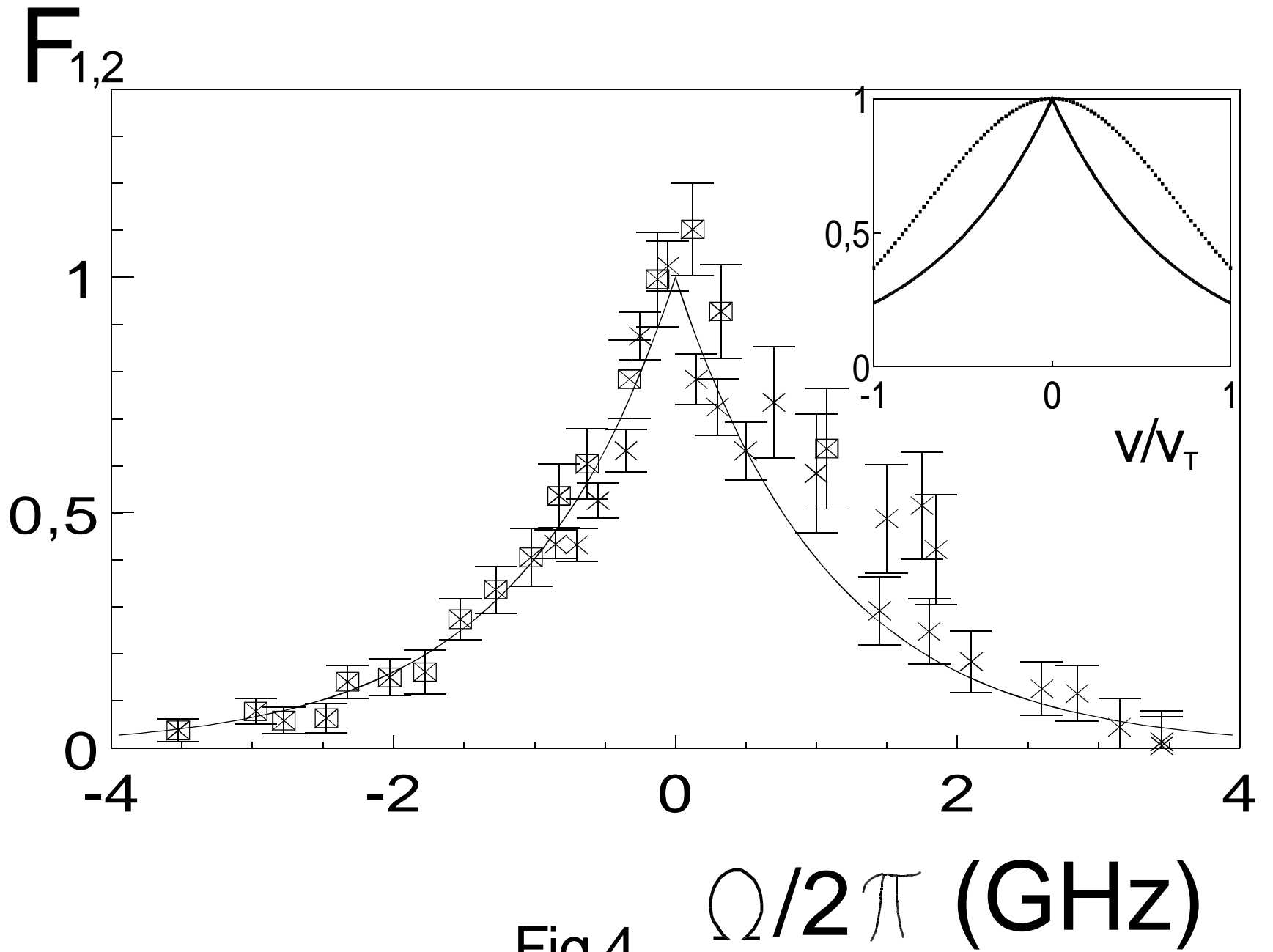


Fig.3



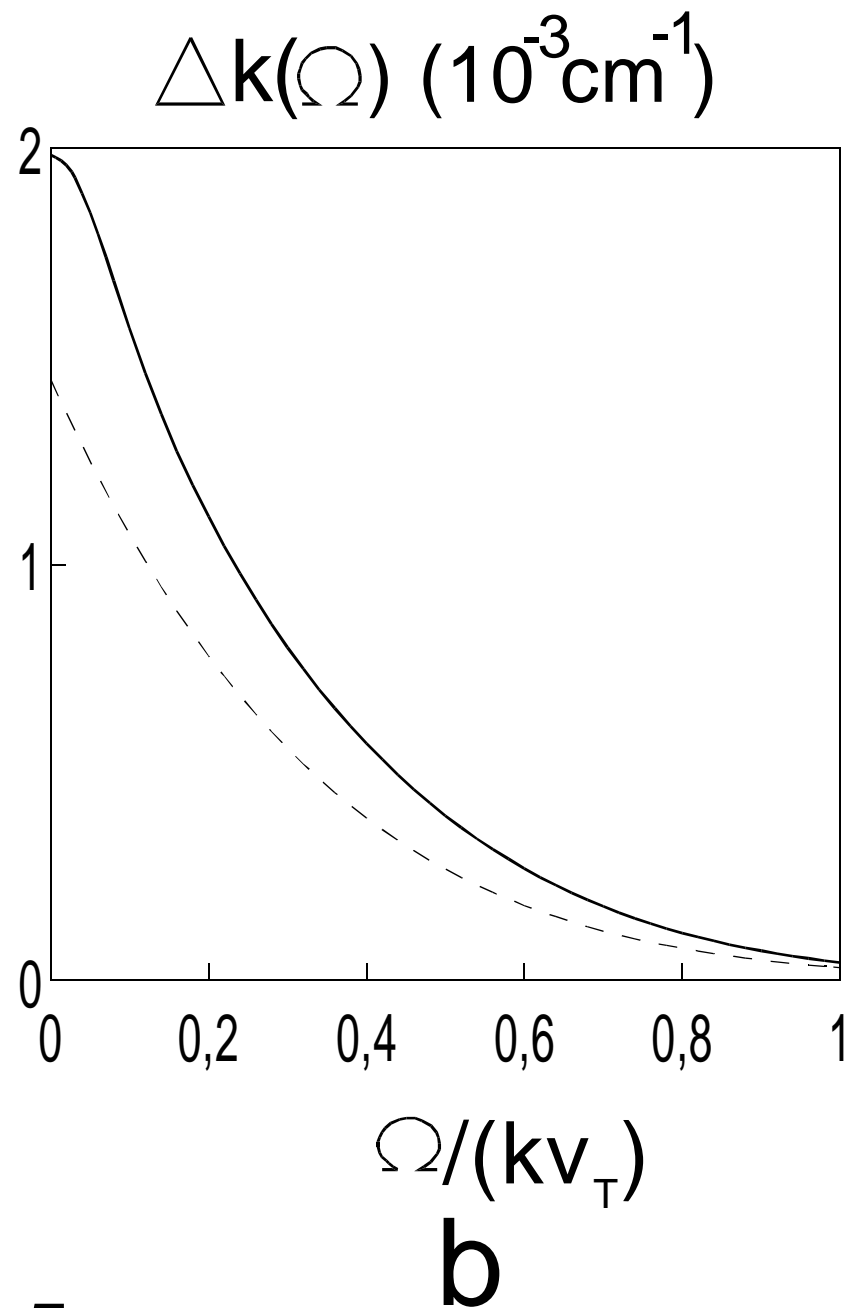
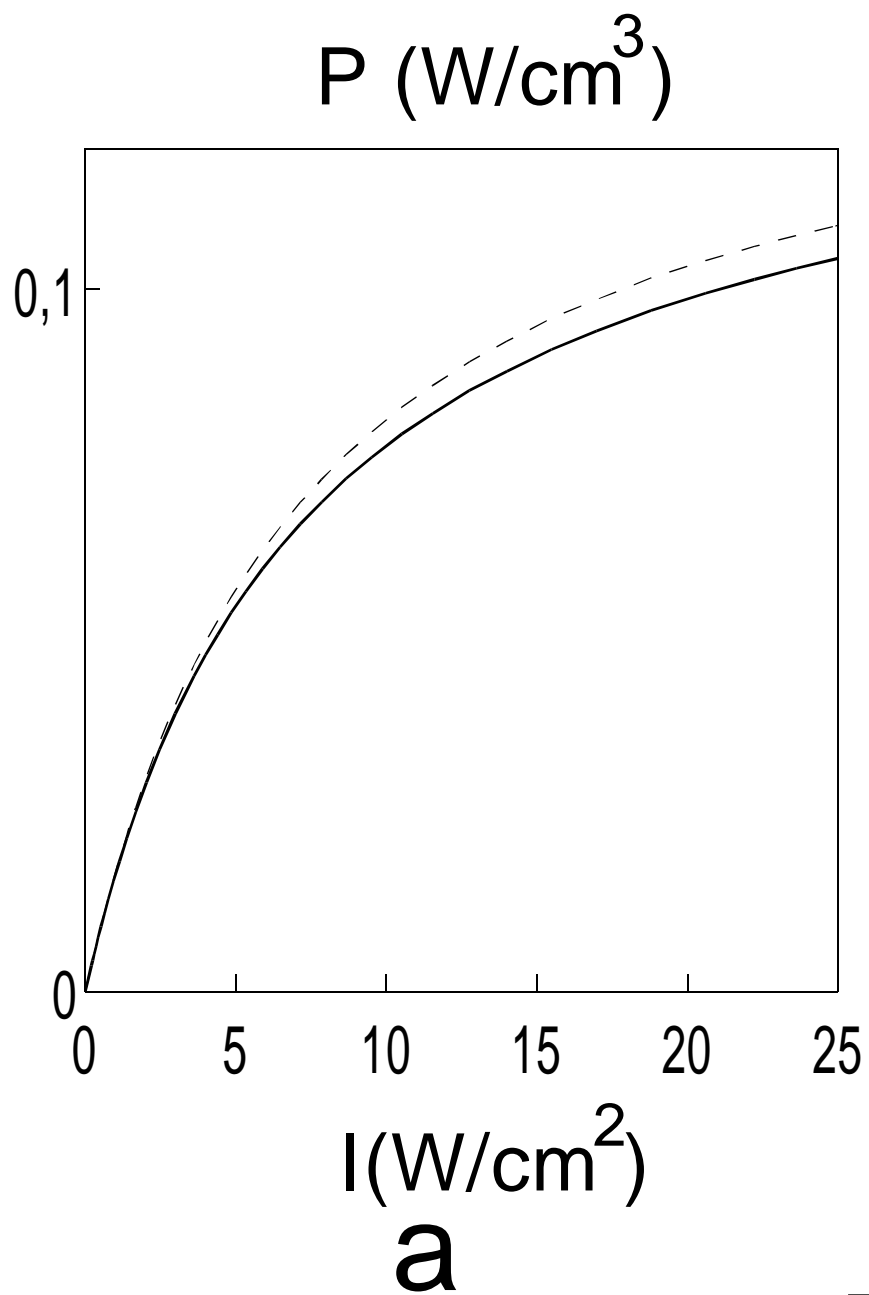


Fig.5